Steel and Composite Structures, *Vol. 33, No. 3* (*2019*) *445-461*
DOI: https://doi.org/10.12989/scs.2019.33.3.445

Transmission of ultrasonic guided wave for damage detection in welded steel plate structures

Xinpei Liu*[1], Brian Uy [1a] and Abhijit Mukherjee [2b]

[1] *School of Civil Engineering, Faculty of Engineering, The University of Sydney, NSW 2006, Australia*
[2] *School of Civil and Mechanical Engineering, Curtin University, Bentley, WA 6102, Australia*

(*Received April 30, 2019, Revised September 28, 2019, Accepted October 18, 2019*)

Abstract. The ultrasonic guided wave-based technique has become one of the most promising methods in non-destructive evaluation and structural health monitoring, because of its advantages of large area inspection, evaluating inaccessible areas on the structure and high sensitivity to small damage. To further advance the development of damage detection technologies using ultrasonic guided waves for the inspection of welded components in structures, the transmission characteristics of the ultrasonic guided waves propagating through welded joints with various types of defects or damage in steel plates are studied and presented in this paper. A three-dimensional (3D) finite element (FE) model considering the different material properties of the mild steel, high strength steel and austenitic stainless steel plates and their corresponding welded joints as well as the interaction condition of the steel plate and welded joint, is developed. The FE model is validated against analytical solutions and experimental results reported in the literature and is demonstrated to be capable of providing a reliable prediction on the features of ultrasonic guided wave propagating through steel plates with welded joints and interacting with defects. Mode conversion and scattering analysis of guided waves transmitted through the different types of weld defects in steel plates are performed by using the validated FE model. Parametric studies are undertaken to elucidate the effects of several basic parameters for various types of weld defects on the transmission performance of guided waves. The findings of this research can provide a better understanding of the transmission behaviour of ultrasonic guided waves propagating through welded joints with defects. The method could be used for improving the performance of guided wave damage detection methods.

Keywords: ultrasonic guided wave; transmission; weld; steel plate; damage detection; finite element model

1. Introduction

Most steel and composite infrastructure consists of welded joints because welding is an economical and efficient method for producing a permanent joint. In recent years, due to the widespread application of high strength steel (HSS) and stainless steel plates in the construction of high-rise buildings, bridges, stadiums and offshore structures, the amount of welded components in large-scale infrastructure was substantially increased, as all the steel plates are often welded to form built-up sections for different structural members (Joo *et al.* 2015, Lian *et al.* 2015, 2017, Choi and Kwon 2018, Huang *et al.* 2019, Ding *et al.* 2019, Li *et al.* 2019, Theofanous *et al.* 2014, Yang *et al.* 2014, Yuan *et al.* 2014) and welding is unavoidable in the fabrication of all these sections. Accordingly, there is increasing awareness of introducing effective defect and damage identification and up-to-the-minute health surveillance to the welded components in large-scale infrastructure, so as to enhance structural reliability and integrity. Different non-destructive testing techniques have been extensively studied or developed for the inspection of weld qualities (AS/NZS 1554.1 2014, Hellier and Shakinovsky 2012, Halmshaw 1997), such as visual inspection, radiography, magnetic particle examination, liquid penetrant examination, eddy current inspection, infrared thermography method, conventional ultrasonic testing and so on. However, visual inspection heavily relies on the experience of operators, and the conditions of welds cannot be assessed quantitatively. Radiographic inspection is hazardous to operators and not suitable for real-time inspection. Magnetic particle and liquid penetrant examination are not effective for internal or subsurface crack detection. Eddy current measurement is not suitable to be applied for materials with lower electrical conductivity like austenitic stainless steel. Infrared thermography method is an indirect measurement and it is difficult to detect internal defects. Ultrasonic testing is one of the most widely adopted testing methods among all these approaches (Ditchburn *et al.* 1996). But the conventional ultrasonic testing using bulk waves need to scan with a high density of inspection points over the entire area of the welded components, which is very time-consuming (Cawley and Alleyne 1996). Furthermore, there are many cases where the weld is inaccessible and the conventional inspection methods are not practicable.

To circumvent the drawback of these conventional testing techniques, the use of ultrasonic guided waves is a

*Corresponding author, Ph.D.,
E-mail: xinpei.liu@sydney.edu.au
[a] Ph.D., Professor, E-mail: brian.uy@sydney.edu.au
[b] Ph.D., Professor, E-mail: abhijit.mukherjee@curtin.edu.au

http://www.techno-press.org/?journal=scs&subpage=6
ISSN: 1229-9367 (Print), 1598-6233 (Online)

very attractive potential solution. The ultrasonic guided waves can be excited at one point on the structure and can be propagated over considerable distances with the characteristics of low attenuation, fast propagation and high sensitivity to structural defects and damages (Rose 2014, Kundu 2016). In case of plates, these guided waves, which are also called Lamb waves (Su and Ye 2009), produce stresses throughout the plate thickness so the entire thickness of the plate can be interrogated. Thus, the use of ultrasonic guided waves could offer the potential for rapid screening of a line or even a large area and remote inspection of physically inaccessible areas on the structure. The activation and acquisition of guided waves are convenient with inexpensive implementation as well. Surprisingly, few studies have been reported in open literature on using ultrasonic guided waves for the structural weld inspection. Yang and Ume (2017) applied the laser/EMAT ultrasonic (LEU) technique to generate Lamb waves for measuring weld penetration depth in thin structures. The transmission coefficients of Lamb waves in the LEU signals were investigated against varying weld penetration depths. Sargent (2006) discovered an interesting type of feature-guided wave propagating along the weld component itself named "weld-guided waves" and discussed the possibility of adopting it for corrosion detection in welds and heat-affected zones. Juluri *et al.* (2007) and Fan and Lowe (2012) investigated the interaction of weld-guided waves with defects located in the material adjacent to the weld, while Kamas *et al.* (2015) examined the interaction of quasi-Rayleigh wave with damages at inaccessible locations in a welded thick plate-like structure. Lu *et al.* (2011) presented a probability-based damage imaging approach with assistance of an active piezoelectric sensor network to predict the presence and location of slot-like damage in the welding zone of a welded tubular steel structure, a true-scale model of a train bogie frame segment. The development of non-contact non-destructive testing methodology using ultrasonic guided waves for comprehensive inspection of weld components of structural members in large-scale infrastructure are still much needed.

The aim of this paper is to gain specific insight of the transmission characteristics of the ultrasonic guided waves propagating through the welded joints with various types of defects or damages in steel plates, which is a particularly important research investigation to advance further development of damage detection technologies through the transmission of ultrasonic guided waves for the systematic inspection of welded joints. In recent years, the use of numerical simulations has been proven to be a highly effective alternative to study the scattering problem of guided waves (Lowe and Diligent 2002, Lowe *et al*. 2002, Gravenkamp *et al*. 2012, Soleimanpour and Ng 2016, Zuo *et al.* 2017, Yang *et al.* 2019). The numerical simulations not only can provide clear signal information for better understanding of the interactive behaviour of guide waves with defects but also are suitable to be used for extensive parametric studies to avoid the sophisticated specimen fabrication, significant monetary expense and the excessive testing time required for conducting physical experiments. Therefore, a three-dimensional (3D) finite element (FE) model, which is verified against the analytical solutions and the experimental results reported in the literature and is demonstrated to be capable of providing a reliable prediction on the features of the ultrasonic guided wave propagating through steel plates with welded joints and interacting with defects, is established and used for the investigation. The mild steel, HSS and austenitic stainless steel plates with welded joints are taken into account in the model. The validated FE model is used to study the mode conversion and scattering characteristics of ultrasonic guided waves transmitted at the welded joints with different types of common defects. A parametric study is then undertaken to investigate the effects of the basic parameters for different types of weld defects on the transmission performance of guided waves.

2. Description of FE model

2.1 General

A 3D explicit FE model is developed to simulate the ultrasonic guided wave propagation in the steel plate with a welded joint. The schematic diagram of a steel plate with welded joint is shown in Fig. 1(a). The size of the steel plate is 600 mm × 450 mm × 4 mm, which is designed based on the estimated travel times of different potential transmitted and reflected waves in the plate to ensure that the plate is large enough for avoiding wave reflections from the plate boundaries to affect the acquired results in this study. The plate is assembled by two individual plates through a welded joint. It is assumed to be a single-V flat-contour butt weld which is produced by gas metal-arc welding and grinding techniques. The geometric dimensions of the weld follow the requirements of the Australian Standards AS/NZS 1554.1 (2014), AS/NZS 1554.4 (2014) and AS/NZS 1554.6 (2012). The details of the schematic cross-section of the welded joint perpendicular to the welding direction are shown in Fig. 1(b). The commercial FE software ABAQUS (Hibbit *et al.* 2016) is used to model this welded steel plate. In the FE model, both the steel plate and the welded joint are simulated using three-dimensional eight-node reduced integration solid brick elements (C3D8R) with hourglass control. The interfaces between the welded joint and steel plate are simulated using a surface-based coupling constraint provided by ABAQUS, called TIE constraint. Such coupling constraints make the translational and rotational motions as well as all other active degrees of freedom equal for a pair of surfaces, of which one is designated to be the master surface (steel plate surface) and the other to be the slave surface (weld edge surface). For the mesh size, Alleyne and Cawley (1991) recommended the following equation for determining the maximum mesh size in simulating the propagation of a guided wave

$$l_e \leq \frac{\lambda_{min}}{10} \tag{1}$$

where l_e is the maximum mesh size and $\lambda_{\min}$ is the minimum

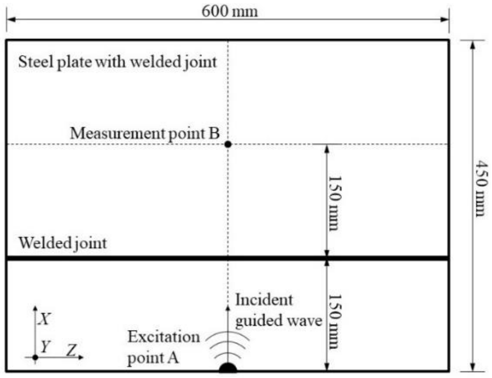

(a) Schematic diagram of steel plate with welded joint

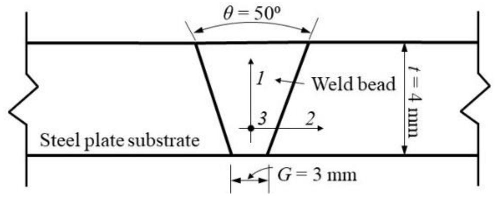

(b) Schematic diagram of cross-section of welded joint

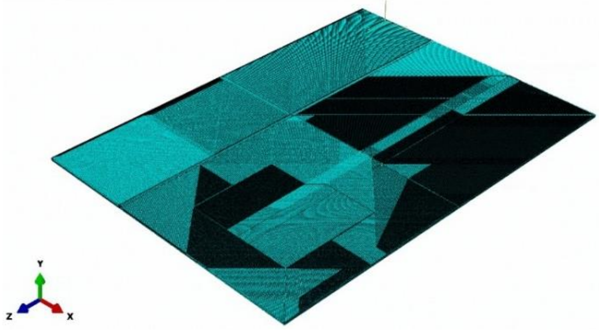

(c) 3D view of FE model with coordinate system

Fig. 1 FE model of steel plate with welded joint

wavelength size in the simulations. The small mesh size used in the FE model satisfies the requirement in Eq. (1) and ensures the accuracy of the simulations. Through sensitivity analysis, approximate mesh size of 0.5 mm is adopted in whole plate model. Fig. 1(c) shows the FE model meshing with the coordinate system.

2.2 Material properties

In this study, the mild steel, HSS and austenitic stainless steel plates with welded joints are under investigation. However, because the density and elastic material properties of the mild steel plate, HSS plate and their corresponding weld components are almost the same, the wave propagation behaviour in these two kinds of plate should also be the same. Accordingly, only the mild steel plate and austenitic stainless steel plate with welded joints will be discussed in the following sections. The material properties of the mild steel plate, normal mild steel weld and the stainless steel plate are considered to be isotopic. The Young's modulus (E), Poisson' s ratio (v) and density (ρ) of these components are assumed to be the same as 200 GPa, 0.3 and 7850 kg/m^2, respectively. On the other hand, 316L industrial austenitic stainless steel welds are adopted for the welded joint of stainless steel plate. Due to the complex process of crystal growing with phase transformations, coarse-grained microstructures usually exist in the austenitic welds with anisotropy (Zhou *et al.* 2018). The behaviour of the ultrasonic waves could be strongly influenced by these highly oriented austenitic welds. Therefore, as suggested by Zhang *et al.* (2006), these austenitic welds can be reasonably considered as transversely isotropic media. The Hooke's law for the austenitic welds is given by

$$[C] = \begin{bmatrix} C_{1111} & C_{1122} & C_{1133} & 0 & 0 & 0 \\ C_{1122} & C_{2222} & C_{2233} & 0 & 0 & 0 \\ C_{1133} & C_{2233} & C_{3333} & 0 & 0 & 0 \\ 0 & 0 & 0 & C_{2323} & 0 & 0 \\ 0 & 0 & 0 & 0 & C_{3131} & 0 \\ 0 & 0 & 0 & 0 & 0 & C_{1212} \end{bmatrix} \tag{2}$$

$$C_{1122} = C_{1133} = 139 \text{ GPa}, C_{2222} = C_{3333} = 233 \text{ GPa}$$

$$C_{2233} = 100 \text{ GPa}, C_{1212} = C_{3131} = 106 \text{ GPa}$$

$$C_{1111} = 194 \text{ GPa}, C_{2323} = \frac{(C_{3333} - C_{2233})}{2} = 65 \text{ GPa}$$

in which the subscripts 1, 2 and 3 represent the three axial directions on the weld as shown in Fig. 1(b).

2.3 Excitation and acquisition

The pulse transmission ultrasonic testing set-up is applied on the steel plate in which the transmission path is perpendicular to the longitudinal direction of the weld bead, as shown in Fig. 1(a). The ultrasonic guided wave is excited at the location A at one end of the plate. The guided wave is excited by applying the nodal displacement to two half circle transducer regions (Soleimanpour and Ng 2016) located at the top and bottom surface of the plate. For the excitation of symmetric guided waves, out-of-plane displacement in opposite directions is applied to the whole surface of the transducer regions at the top and bottom

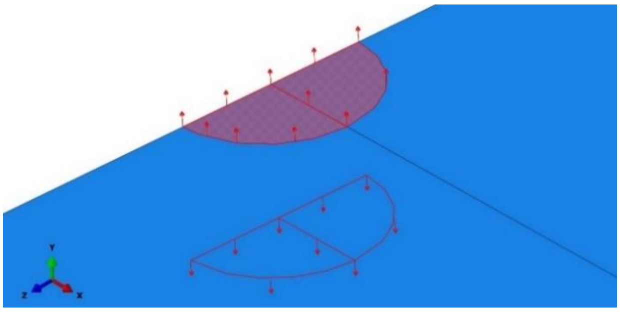

(a) Symmetric mode guided wave

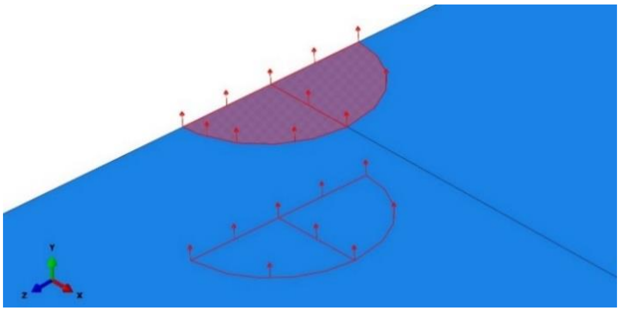

(b) Anti-symmetric mode guided wave

Fig. 2 Excitation of symmetric and anti-symmetric mode guided waves

surfaces, as shown in Fig. 2(a). While for the excitation of anti-symmetric guided waves, out-of-plate displacement in the same direction is applied to the whole surface of the transducer regions at the top and bottom surfaces as shown in Fig. 2(b). The magnitude of the displacement is set to be 1 μm.

The propagating guided wave signals are obtained at the measurement points. The symmetric guided waves are measured through monitoring the in-plane displacement (in the *x*-axis) of nodes located at the mid-thickness of the plate. This ensures that only the symmetric guided waves are detected since the anti-symmetric and shear horizontal guided waves at certain frequency exhibit zero in-plane displacement of the nodes located at mid-thickness. The anti-symmetric guided waves are measured through monitoring the out-of-plane displacement (in the *y*-axis) of nodes located at the mid-thickness of the plate, thus ensuring that only the anti-symmetric propagating modes are detected, since the symmetric and shear horizontal guided waves at certain frequency have zero out-of-plane displacement at this depth. The out-plane displacement on the plate surface at the measurement points is also recorded throughout the signal monitoring process for checking purposes.

2.4 Dynamic analysis

The dynamic analysis is solved using the explicit FE code in ABAQUS, which uses the central-difference integration scheme. In this scheme, the integration operator matrix is inverted, and a set of nonlinear equilibrium equations is solved at each time increment. As the central different integration scheme is conditionally stable, the increment time step needs to be small enough to ensure computational stability. Stewart *et al.* (2006) recommended limiting the hourglass energy to less than 2 % of the total energy to ensure the accuracy of predicting the guided wave propagation in solids. Bathe (1982) recommended the following condition to ensure the stability of the explicit analysis

$$D_t \leq \frac{L_{min}}{c_{max}} \tag{3}$$

where D_t is the time increment, $L_{\min}$ is the smallest mesh size in the finite element model and $c_{\max}$ is the longitudinal wave velocity in the plate. However, the time increment is automatically determined by ABAQUS for all simulations in this study.

3. Validation of FE model

3.1 Analytical verification

The FE model is firstly validated by comparing its predicted results of the phase velocity, group velocity and mode shape of the symmetric and anti-symmetric guided waves with the semi-analytical results calculated by GUIGUW software (Marzani *et al.* 2008) based on semi-analytical finite element (SAFE) formulations. In this part of the study, there are no welded joints and defects in the steel plate. A narrow-band 5-cycle sinusoidal tone burst pulse modulated by Hanning window with a central frequency chosen from 50 kHz to 400 kHz with steps of 50 kHz is applied for generating the ultrasonic guided wave. Because the excitation frequencies are below the cut-off frequency (Su and Ye 2009), only fundamental symmetric mode (S_0) and anti-symmetric mode (A_0) guided waves are generated except for the shear mode wave. In this FE simulation, the signals of S_0 and A_0 guided waves are recorded at 10 measurement points with 2 mm distance away from each other along one line on the plate. The captured data is used to calculate the group and phase wave velocities at different excitation frequencies. The phase velocity c_p of the guided wave on plate can be calculated (Soleimanpour and Ng 2015) by

$$c_p = \frac{2\pi f}{k} = \frac{2\pi f \Delta x}{\Delta \varphi} \tag{4}$$

where f is the central frequency of the incident wave, k is the rate of phase change at a certain distance, $\Delta\phi$ is the phase change corresponding to measurement points with a distance Δx that is less than a wavelength. Thus, the phase velocity is obtained by calculating the phase change of the signals between two measurement points and then substituting them into Eq. (4). The group velocity c_g of the guided wave on the plate can be calculated by

$$c_g = \frac{\Delta x}{\Delta t} \tag{5}$$

where Δt is the difference of the wave packet arrival times between two measurement points with a distance Δx. The arrival time of the wave packet signal is calculated from a signal envelope obtained by the Hilbert transform (Staszewski *et al.* 2004). The Hilbert transform is defined as

$$H(t) = \frac{1}{\pi}\int_{-\infty}^{+\infty}\frac{f(\tau)}{t-\tau}d\tau \tag{6}$$

where $H(t)$ is the Hilbert transform of signal $f(t)$. Eq. (6) performs a 90° phase shift or quadrature filter to construct a so-called analytic single $F_A(t)$

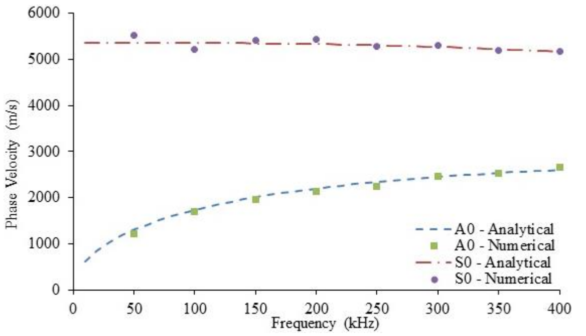

Fig. 3 Comparison of phase velocity dispersion curves for 4 mm thick steel plate obtained from finite element model and semi-analytical solutions

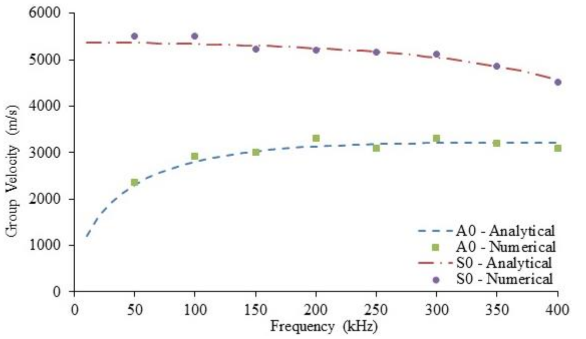

Fig. 4 Comparison of group velocity dispersion curves for 4 mm thick steel plate obtained from finite element model and semi-analytical solutions

$$F_A(t) = f(t) + iH(t) = e(t)e^{i\varphi(t)} \tag{7}$$

in which

$$e(t) = \sqrt{f^2(t) + H^2(t)} \tag{8}$$

and

$$\varphi(t) = \frac{1}{2\pi}\frac{d}{dt}arctan\frac{H(t)}{f(t)} \tag{9}$$

where $e(t)$ is the module of $F_A(t)$ and its envelope depicts the energy distribution of $f(t)$ in the time domain. The phase and group velocity of the guided wave at each frequency are obtained by averaging the calculated velocities from these 10 measurement point results. Figs. 3 shows the comparisons of the phase velocity dispersion curves for 4 mm thick steel plate calculated by the FE simulations and semi-analytical solution for the S_0 and A_0 guided waves, while Fig. 4 depicts the comparisons of the group velocity dispersion curves. Figs. 5 and 6 show the comparisons of the mode shapes of 300 kHz S_0 and A_0 guided waves for 4 mm thick steel plate obtained from the FE model and semi-analytical solution, respectively. It can be seen that the results obtained from the FE model and the semi-analytical results show a very good agreement. Therefore, it has been verified that the FE model is capable of accurately simulating the propagation of various guided waves at different excitation frequencies in the steel plate.

3.2 Experimental verification

To further validate accuracy of the FE model, the developed FE model is used for modelling the tests of transmitting ultrasonic guided waves for inspecting steel plates with various notch depths. The details of this experiment are given in the reference (Alleyne and Cawley 1992). The steel plates in the experiment were 3 mm thick and approximately 300 mm wide and 1 m long. Five plates were tested, one having no notch and the other having 0.5 mm wide notches milled across the full plate width along the welding direction and normal to the transmission path used. Plates with notches 0.5, 1.0, 1.5 and 2.0 mm depth were tested. A 12 cycles and 480 kHz toneburst modified by

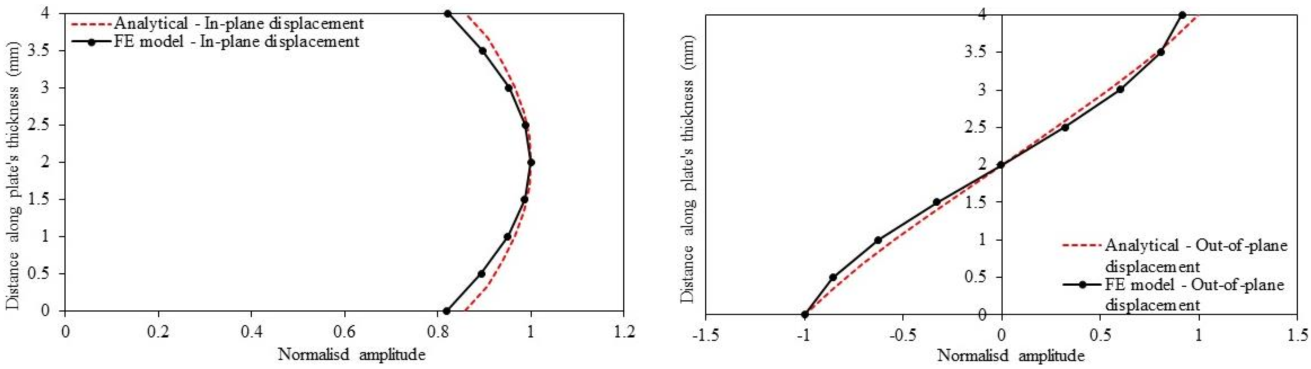

(a) In-plane displacement (in the x-axis) (b) Out-of-plane displacement (in the y-axis)

Fig. 5 Comparison of mode shapes of 300 kHz S0 mode guided wave for 4 mm thick steel plate obtained from finite element model and semi-analytical solution

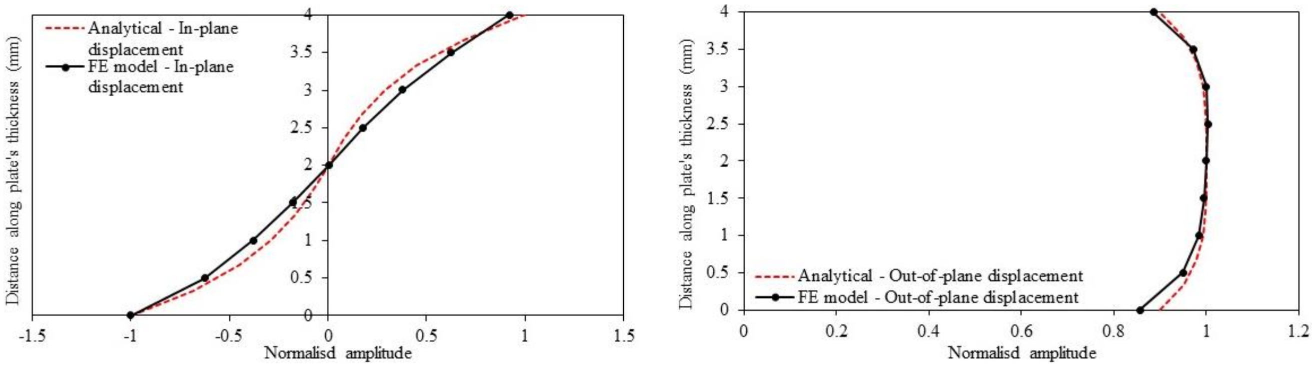

(a) In-plane displacement (in the *x*-axis)

(b) Out-of-plane displacement (in the *y*-axis)

Fig. 6 Comparison of mode shapes of 300 kHz A_0 mode guided wave for 4 mm thick steel plate obtained from finite element model and semi-analytical solution

Table 1 Comparison of the peak to peak amplitude ratio of S_0 guided wave signals from tests and FE analysis

Notch depth	Signal peak to peak amplitude ratio		A_{FE}/A_{test}
	Experimental results A_{test}	FE results A_{FE}	
1/6 plate thickness	0.98	0.983	1.003
1/3 plate thickness	0.82	0.819	0.999
1/2 plate thickness	0.59	0.561	0.951
2/3 plate thickness	0.39	0.368	0.943
		Mean	0.974
		COV	0.032

Hanning window was employed to generate the S_0 guided wave. The notch and the signal receiver are located at distance of 250 and 350 mm from the transmitter, respectively. The peak to peak amplitude ratio of transmitted S_0 wave signal was obtained by dividing the maximum amplitude of the signal received in the steel plate with notch by the maximum amplitude of the reference signal received in the steel plate without any notch. Table 1 presents the comparisons of the peak to peak amplitude ratio obtained from the tests and from the FE analysis. It can be seen that the mean value of the ratio of the numerical result to experimental result is 0.974 with the coefficient of variation (COV) being 3.2%. Both results show good agreement. It is demonstrated that the FE model can predict the propagation of ultrasonic guided waves in a steel plate with defects and capture rationally the interaction of ultrasonic guided waves with a defect in the plate.

3.3 Guided wave propagation in welded steel plate

The aim of this section is to illustrate the capacity of the developed FE model for simulating the wave propagation in steel plates with welded joints. The ultrasonic guided wave propagation in three different steel plates, viz. a mild steel plate in the absence of a welded joint, a mild steel plate with a welded joint and an austenitic stainless steel plate with a welded joint, are modelled for comparison. The material properties and geometric dimensions of the plate

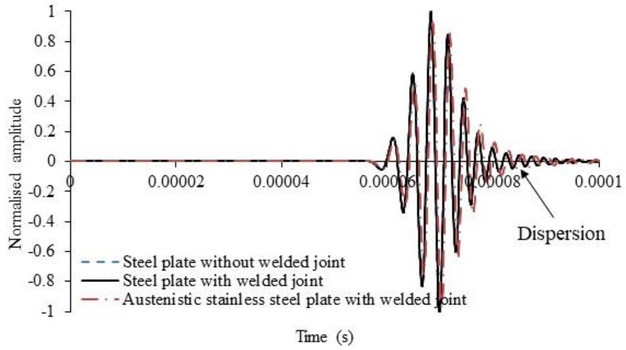

Fig. 7 Signal of S_0 guided waves received at 300 mm from the excitation point

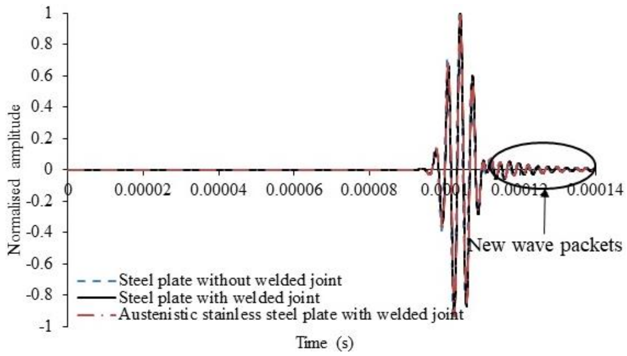

Fig. 8 Signal of A_0 guided waves received at 300 mm from the excitation point

have been described in Section 2. A 5-cycle sinusoidal tone burst pulse modulated by Hanning window with central frequency of 300 kHz is applied for generating the S_0 and A_0 guided waves. Fig. 7 shows the received signal of S_0 guided waves for the measurement point B located at a distance of 300 mm from the excitation point A or at a distance of 150 mm from the mid-width point of a welded joint. In the figure, the amplitude of the wave signal is normalised by the maximum absolute amplitude of the signal in the corresponding figure for better illustration purposes, which is also applicable to most of the figures in this paper. It can be seen from Fig. 7 that the received signal of S_0 guided wave in the mild steel plate without welded joint overlap completely with the one in the mild steel plate with welded joint. This is because these two plate models have the same material properties and the same geometric dimensions as a whole plate although the plate assemblies are different. The obtained results illustrate the accuracy of the steel plate with welded joint model for simulating the S_0 guided wave propagation. For the austenitic stainless steel plate with welded joint, only a small phase shift and amplitude change on the received time-domain signal output, caused by the elastic anisotropy of austenitic welds, can be observed when compared with those of the other two plates. This highlights the advantage of using ultrasonic guided waves for weld defect detection against the use of ultrasonic bulk wave which is often difficult as the ultrasonic beam could become distorted with severe scattering and attenuation when propagating into the austenitic welds (Zhou *et al.* 2018). It should be noted that, as is shown in Fig. 7, the S_0 guided wave may disperse after traveling considerable distance due to the dispersive characteristic of the S_0 guided wave at a central frequency of 300 kHz as indicated in the dispersion curve shown in Fig. 4. Fig. 8 displays the received signal of A_0 guided waves for the measurement point B. Three received signals of A_0 guided waves in the mild steel plate without welded joint, mild steel plate and the austenitic stainless steel plate with welded joint are almost identical. This not only validates the accuracy of the FE model for simulating the A_0 mode wave propagation in steel plate with welded joint but also indicates that the anisotropic properties of austenitic welds may have little effect on the propagation of A_0 mode guided wave in healthy welded steel plate. In addition, it is noted from Fig. 8 that when generating the A_0 guide wave in the plate with finite cross-section, there could be new anti-symmetric mode wave packets generated following the incident A_0 wave travelling throughout the plate. This phenomenon has been reported in the literature (Serey *et al.* 2018) which provided the experimental observation. Thus, the results obtained from this three-dimensional FE model could be more accurate than those obtained from the conventional two-dimensional model for simulating ultrasonic guided wave propagation.

4. Mode conversion and scattering analysis

4.1 Types of weld defects

In this section, the verified FE model is used to study the mode conversion and scattering characteristics of ultrasonic guided waves transmitted at various types of weld defects in steel plates. The material properties and geometric dimensions of the steel plates and welded joints are the same as the ones described in Section 2. The pulse transmission ultrasonic testing set-up is applied in the model as shown in Fig. 1(a). The guided wave is excited in point A located at one end of the plate. The distance between the excitation point A and the mid-width point of the welded joint is 150 mm which is more than five wavelengths that fulfils the far-field wave field solution requirement (Fan and Lowe 2012, Moreau and Castaings 2008). The distance between the mid-width point of welded joint and the measurement point B is also set to be 150 mm to ensure the possible transmitted and converted waves after interacting with weld defect can be separated. The excitation signal is a narrow-band 5-cycle sinusoidal tone burst pulse modulated by Hanning window with central frequency at 300 kHz. The S_0 and A_0 guided wave are used individually as incident wave in the tests.

Five types of common weld defects (Hellier and Shakinovsky 2012, Stavridis *et al.* 2018, Consonni *et al.* 2012, Murta *et al.* 2018) viz. toe crack, root crack, lack-of-penetration, porosity and lack-of-fusion as shown in Fig. 9 are considered in this study. In the FE model, simulated artificial discontinuities corresponding with each type of common defect are introduced into the welded steel plate.

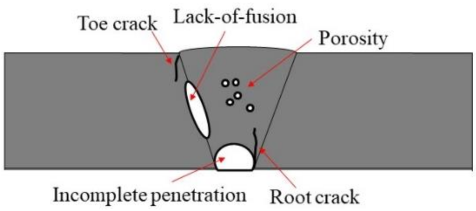

Fig. 9 Possible defects in welded joints

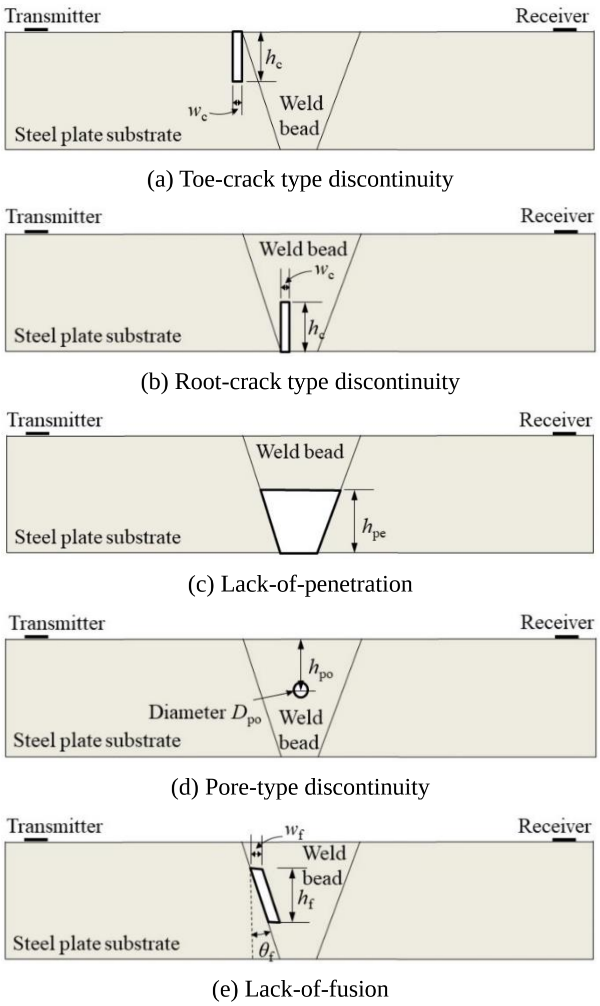

Fig. 10 Simulated defects in welded joints

The schematic diagrams of the cross-section of welded joint with simulated artificial discontinuity are shown in Fig. 10. Straight sided notches in the welded steel plates are investigated in the FE model as they are a reasonable idealisation of crack-type defect. The toe and root crack defects (Figs. 10(a) and (b)) are defined by notches next to the edge of the weld bead on the top surface of base material and on the bottom surface of weldment, respectively. The depth h_c and width w_c of notch for 4 mm thick plate are 2 and 0.5 mm, respectively. Lack-of-penetration, porosity and lack-of-fusion are the common weld defects recognised in the welding process. Lack-of-penetration is a weld defect found at the backwall of a weld bead. A trapezoidal shape notch-like discontinuity (Fig. 10(c)) with a depth h_{pe} of 2 mm is introduced at the root of weld for modelling this type of defect. A circular void (Fig. 10(d)) with a diameter D_{po} of 1 mm is inserted inside the weldment section for modelling the porosity defect. The distance h_{po} between the centre of circle and the top surface of plate is 2 mm. The lack-of-fusion defect is a kind of defect that is geometrically similar to a crack and could initiate fatigue cracking during component use. This defect is achieved by inserting an internal inclined discontinuity (Fig. 10(e)) with a height h_f of 2 mm, width w_f of 0.5 mm and inclined angle θ_f of 25° at the surface of weldment to the base material substrate. The central point of this discontinuity is at the mid-thickness point of the plate. It should be noted that in the FE models, all types of simulated artificial discontinuities are defined to be cut through the full width of the plate along the welding direction for simplifying the comparison.

4.2 S_0 wave incident

One set of tests are carried out to investigate the mode conversion and scattering characteristics of guided waves transmitted at various types of weld defects when the incident wave is S_0 guided wave. Fig. 11 shows typical time snapshots of the contour of the magnitude of out-of-plane displacement from the FE simulation of the incident S_0 wave propagating through a steel welded joint with toe crack. Fig. 11(a) clearly shows that the S_0 guided wave is properly excited while the interaction of the guided wave with the welded joint with defect is shown in Fig. 11(b). As is displayed in Fig. 11(c), followed by the wave interacting with the weld defect, two propagating modes of waves including the transmitted S_0 wave and converted A_0 wave are present on the plate. After traveling considerable distance, two propagating modes of waves are separated as depicted in Fig. 11(d). Fig. 12 shows the signals of the transmitted S_0 wave and converted A_0 wave received at the measurement point B. The arrival time of each wave packet can be calculated by determining wave envelope through Hilbert transform. The arrival time of the transmitted S_0 wave packet at the measurement point B is calculated as 57.8 μs. The theoretical arrival time of the incident S_0 wave at this measurement point is 59.5 μs, which agrees with the FE results. Similarly, the theoretical arrival time of the converted A_0 wave from weld defect is 76.5 μs which also agrees with the calculated FE result of 75.8 μs. It indicates that two propagating modes of waves indeed exist after the incident S_0 guided wave interacting with weld defect and have separated at the measurement point B. Fig. 13 shows the comparison of the transmitted S_0 wave signals measured at point B after propagating through the healthy welded joint and welded joint with toe crack. It is shown that the maximum amplitude of S_0 wave signal for the welded steel plate with toe crack is reduced by 36.7 % compared with the one for the healthy welded plate, which means the S_0 guided wave is very sensitive to this type of defect. Figs.

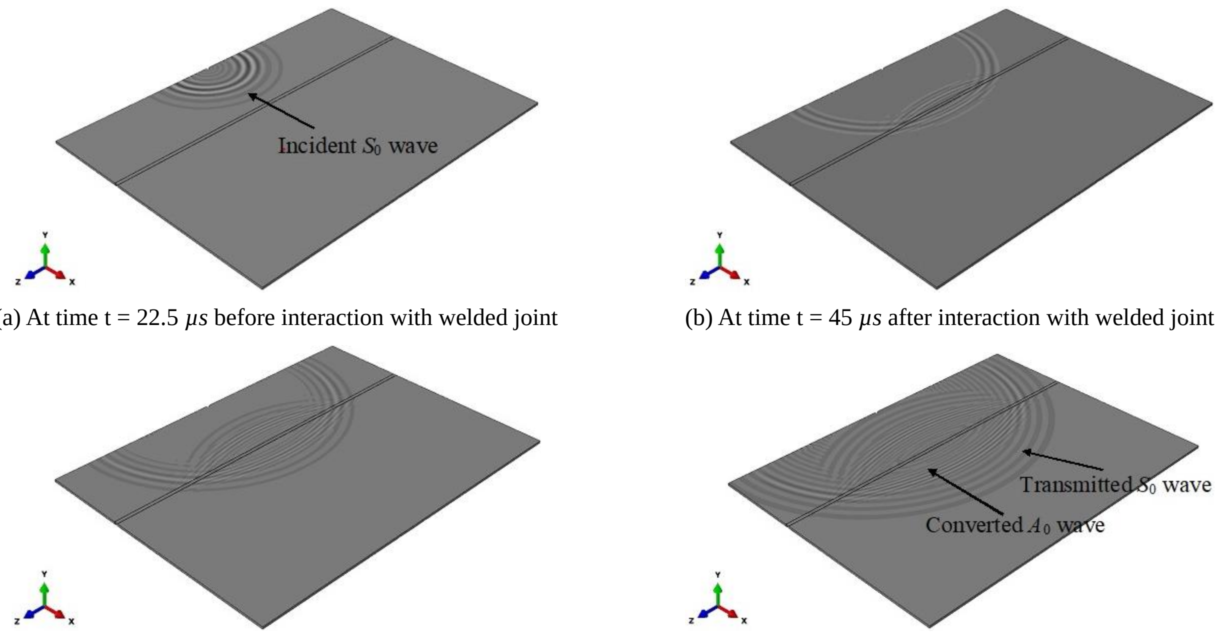

(a) At time t = 22.5 μs before interaction with welded joint

(b) At time t = 45 μs after interaction with welded joint

(c) At time t = 52.5 μs when the transmitted S_0 and converted A_0 waves start to separate

(d) At time t = 60 μs when the transmitted S_0 and converted A_0 waves almost separate

Fig. 11 Snapshots for mode conversion of incident S_0 wave propagating through steel welded joint with toe crack

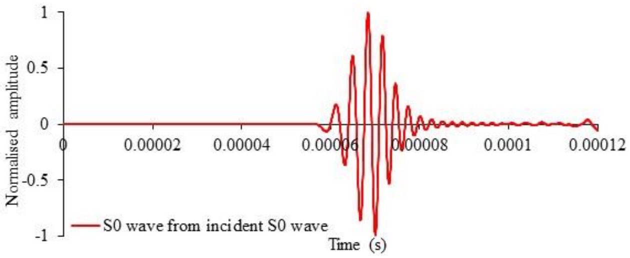

(a) S_0 wave from incident S_0 wave

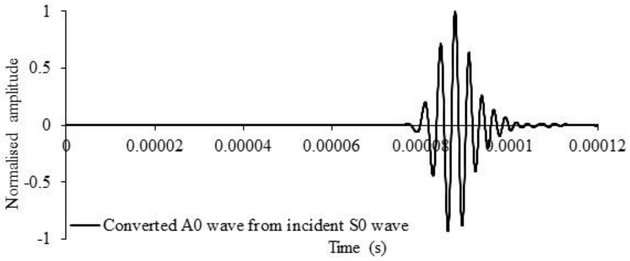

(b) Converted A_0 wave from incident S_0 wave

Fig. 12 Mode conversion of incident S_0 wave propagating through steel welded joint with toe crack

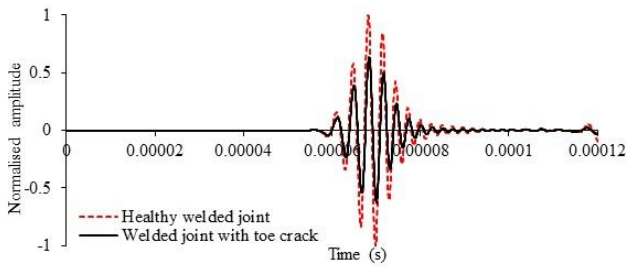

Fig. 13 Comparison of signals of S_0 wave after propagating through welded joint without and with toe crack

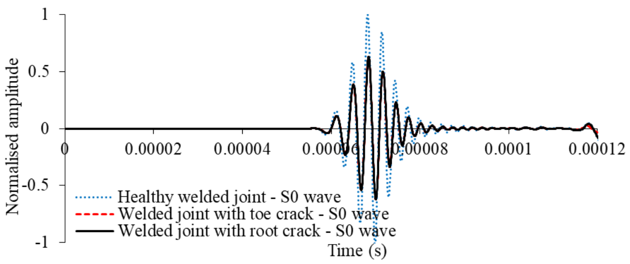

(a) S_0 wave from incident S_0 wave

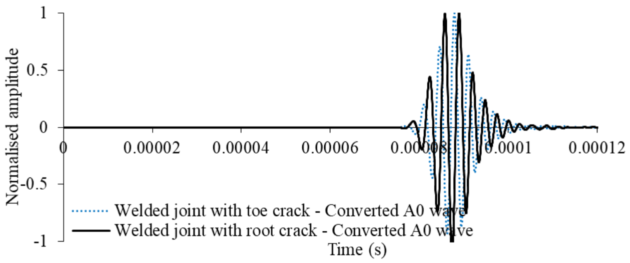

(b) Converted A_0 wave from incident S_0 wave

Fig. 14 Mode conversion of incident S_0 wave propagating through steel welded joint with root crack

14-17 shows the signals of the transmitted S_0 wave and converted A_0 wave received at the measurement point B from the FE simulation of incident S_0 guided wave propagating through steel welded joint with the defects of root crack, lack-of-penetration, porosity and lack-of-fusion, respectively. As is shown in Fig. 14, the received transmitted S_0 wave signals for the toe crack and root crack cases are identical because the geometric dimensions of the simulated toe crack and root crack are the same. While small phase shift between the converted A_0 wave signals for the toe crack and root crack cases can be recognised, which is due to the difference of the crack locations. Fig. 15 illustrates that the received signals of S_0 guided waves

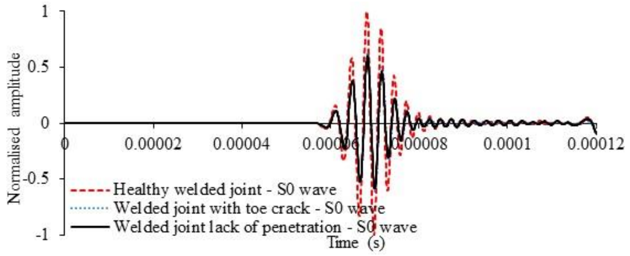

(a) S_0 wave from incident S_0 wave

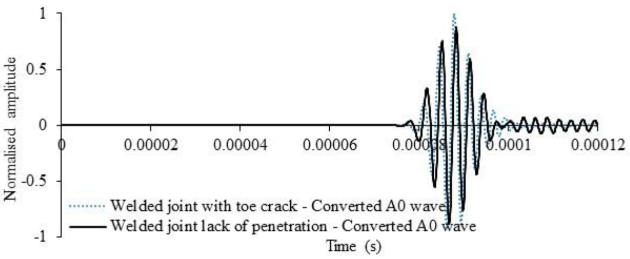

(b) Converted A_0 wave from incident S_0 wave

Fig. 15 Mode conversion of incident S_0 wave propagating through steel welded joint lack of penetration

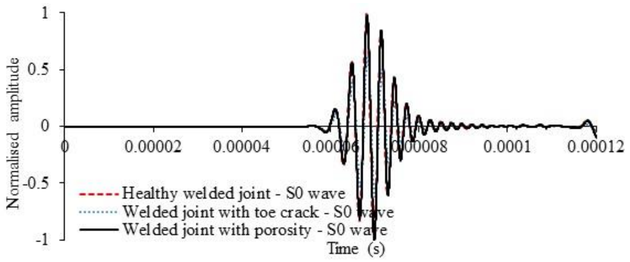

(a) S_0 wave from incident S_0 wave

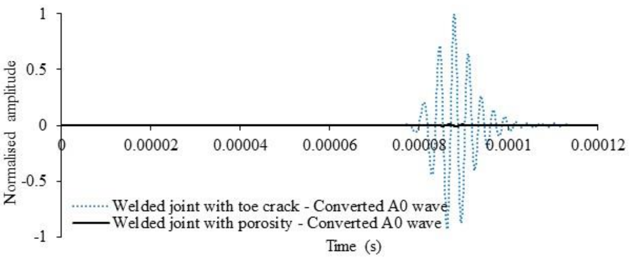

(b) Converted A_0 wave from incident S_0 wave

Fig. 16 Mode conversion of incident S_0 wave propagating through steel welded joint with porosity

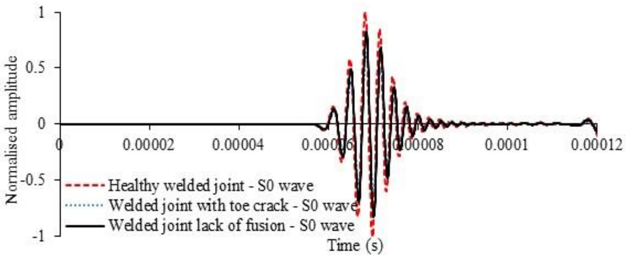

(a) S_0 wave from incident S_0 wave

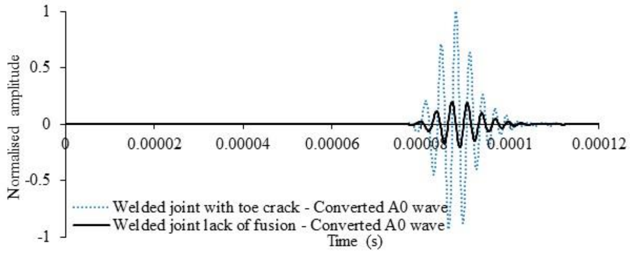

(b) Converted A_0 wave from incident S_0 wave

Fig. 17 Mode conversion of incident S_0 wave propagating through steel welded joint lack of fusion

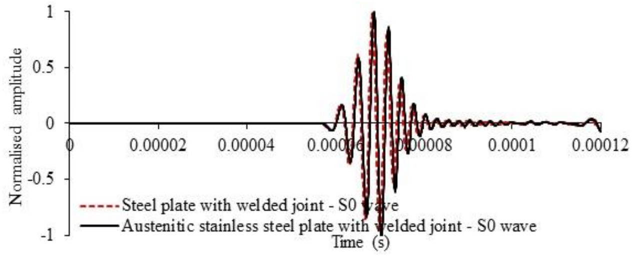

(a) S_0 wave from incident S_0 wave

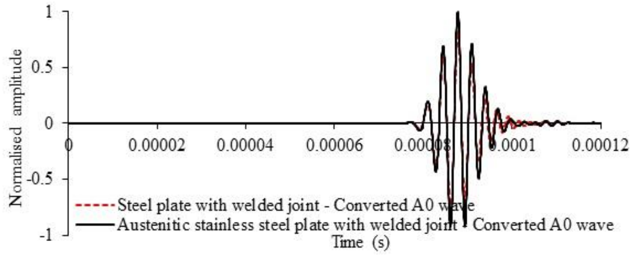

(b) Converted A_0 wave from incident S_0 wave

Fig. 18 Comparison of signals from incident S_0 wave after propagating through mild steel plate and austenitic stainless steel plate with welded joints

propagating through welded joints with toe crack and with lack-of-penetration defect are very similar, since the notch-like discontinuity is made for modelling the lack-of-penetration defect even though the shape of cross-section of this notch-like discontinuity is trapezoidal rather than rectangle. It can be observed from Fig. 16 that the S_0 guided wave is not sensitive to the pore-type defect as the loss of the magnitude of S_0 wave signal after the interaction with the defect is negligible and the converted A_0 wave signal is barely detected. Similar observations can be realised on the signal for the lack-of-fusion case as shown in Fig. 17, which could be due to the location of both types of defects which is located internally around the mid-thickness of the plate. However, the loss of the magnitude of the transmitted S_0 wave signal for the lack-of-fusion defect case could be slightly more severe and the converted A_0 wave signal are much more obvious compared with those for the porosity case, which could be caused by the larger size of the lack-of-fusion defect. The comparison of the received signals from the FE simulation of the incident S_0 wave propagating through the mild steel plate and austenitic stainless steel

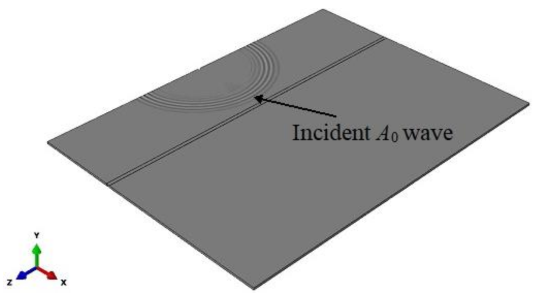

(a) At time t = 45 μs before interaction with welded joint

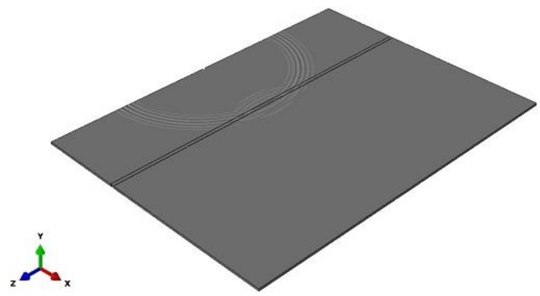

(b) At time t = 60 μs after interaction with welded joint

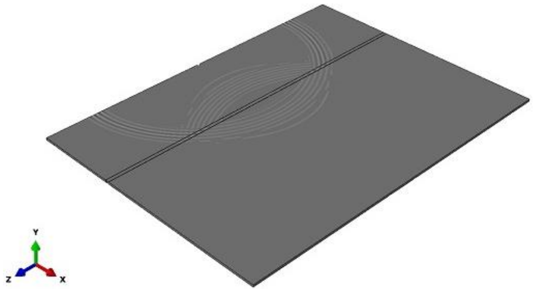

(c) At time t = 75 μs when the transmitted S_0 and converted A_0 waves start to separate

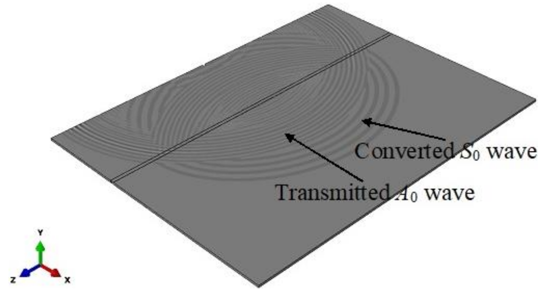

(d) At time t = 90 μs when the transmitted S_0 and converted A_0 waves almost separate

Fig. 19 Snapshots for mode conversion of incident A_0 wave propagating through steel welded joint with toe crack plate with the welded joints is depicted in Fig. 18. The integrity of the signals of the waves propagating through two kinds of plates is almost the same although attention may need to be paid on the amplitude of the received signals.

4.3 A_0 wave incident

Another set of tests are carried out to investigate the mode conversion and scattering characteristics of guided waves transmitted at various types of weld defects when the incident wave is A_0 guided wave. Similar as is discussed in Section 4.2 on S_0 wave incident, Fig. 19 shows typical time snapshots of the contour of the magnitude of out-of-plane displacement from the FE simulation of the incident A_0 guided wave propagating through a steel welded joint with toe crack. It is indicated from Fig. 19 that after the incident A_0 wave interacting with the weld defect, two propagating modes of waves including the transmitted A_0 wave and converted S_0 wave are generated. Fig. 20 shows the signals of the transmitted A_0 wave and converted S_0 wave received at the measurement point B. The theoretical arrival time of the incident A_0 wave and converted S_0 wave at this measurement point are 93.6 and 76.5 μs, respectively, which agree with the FE results of 95.1 and 76.0 μs. The comparison of the transmitted A_0 wave signals measured at point B after propagating through the healthy welded joint and welded joint with toe crack is depicted in Fig. 21. It is observed that the shape of the transmitted A_0 wave packet after propagating through the weld defect has been changed and is slightly different than the one in the healthy steel plate. It may be because of the reconstruction of the incident A_0 wave packet with the new anti-symmetric mode wave packets mentioned in Section 3.3 after interacting with the weld defect. The maximum amplitude of A_0 wave signal is reduced by 47.3 % for the welded steel plate with toe crack compared with the one for the healthy welded

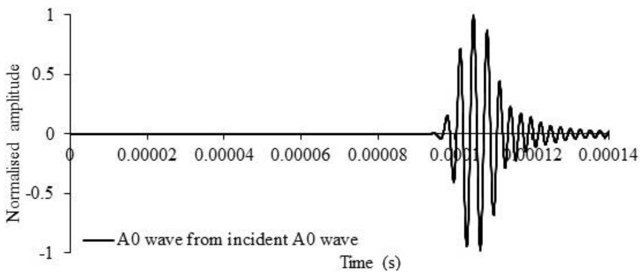

(a) A_0 wave from incident A_0 wave

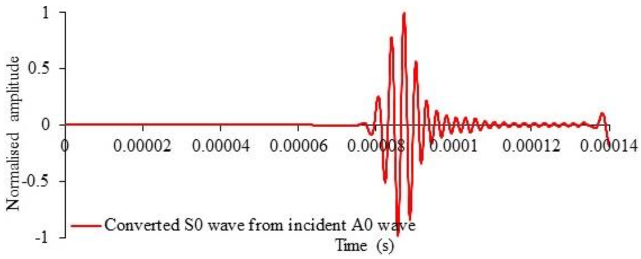

(b) Converted S_0 wave from incident A_0 wave

Fig. 20 Mode conversion of incident A_0 wave propagating through steel welded joint with toe crack

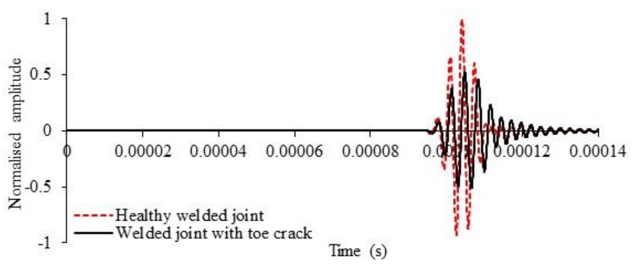

Fig. 21 Comparison of signals of A_0 wave after propagating through welded joint without and with toe crack

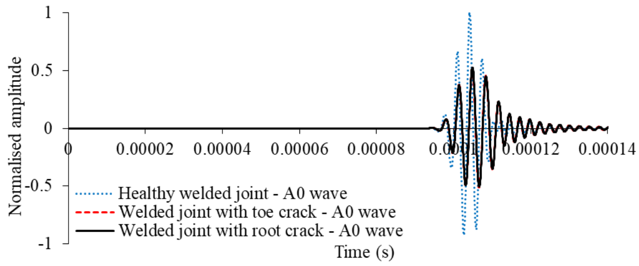

(a) A_0 wave from incident A_0 wave

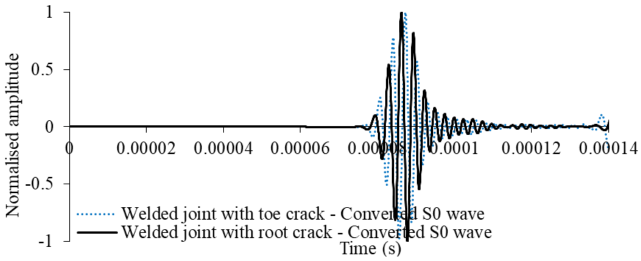

(b) Converted S_0 wave from incident A_0 wave

Fig. 22 Mode conversion of incident A_0 wave propagating through steel welded joint with root crack

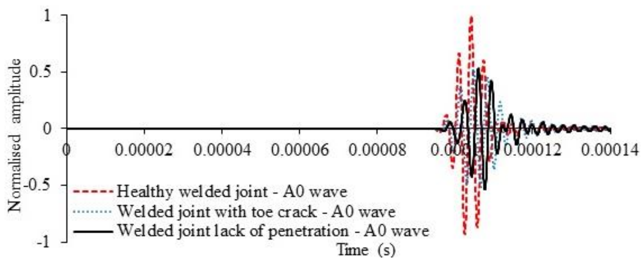

(a) A_0 wave from incident A_0 wave

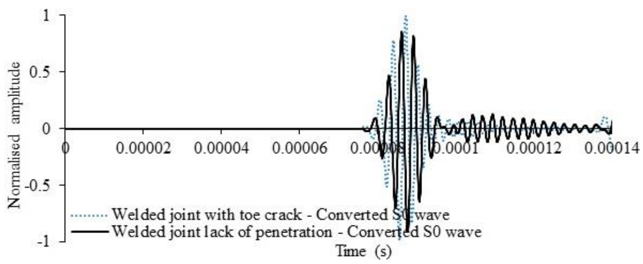

(b) Converted S_0 wave from incident A_0 wave

Fig. 23 Mode conversion of incident A_0 wave propagating through steel welded joint lack of penetration

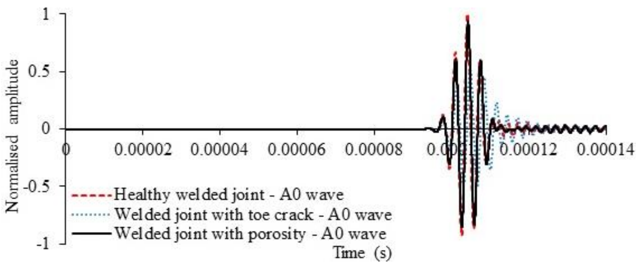

(a) A_0 wave from incident A_0 wave

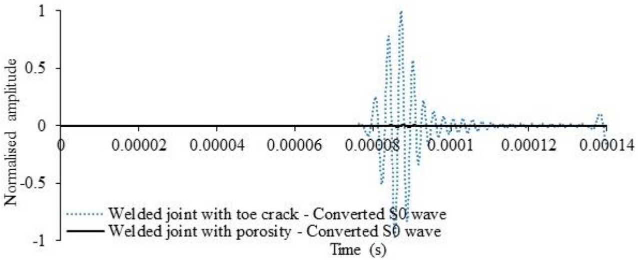

(b) Converted S_0 wave from incident A_0 wave

Fig. 24 Mode conversion of incident A_0 wave propagating through steel welded joint with porosity

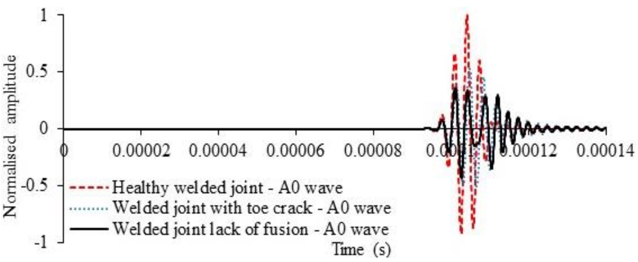

(a) A_0 wave from incident A_0 wave

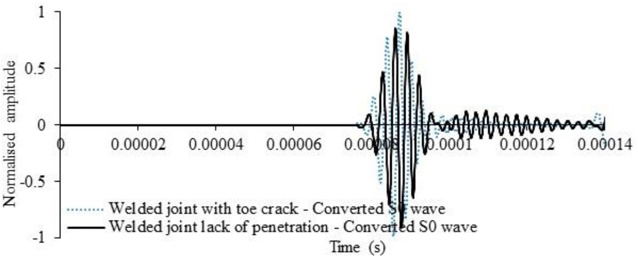

(b) Converted S_0 wave from incident A_0 wave

Fig. 25 Mode conversion of incident A_0 wave propagating through steel welded joint lack of fusion

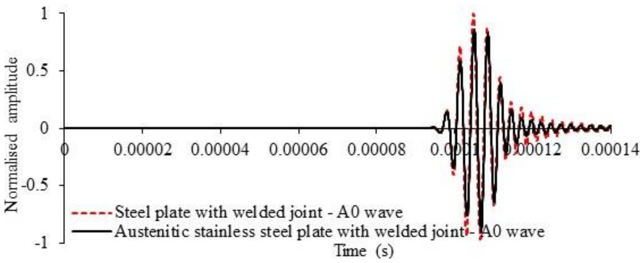

(a) A_0 wave from incident A_0 wave

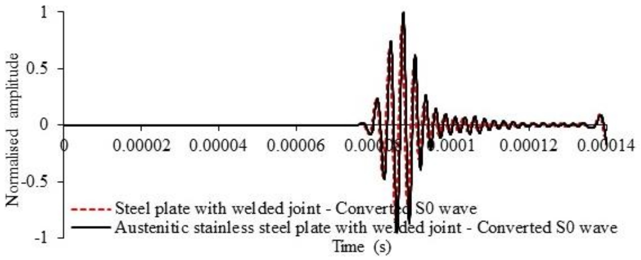

(b) Converted S_0 wave from incident A_0 wave

Fig. 26 Comparison of signals from incident A_0 wave after propagating through mild steel plate and austenitic stainless steel plate with welded joints

plate, which also demonstrates the sensitivity of A_0 guided waves to this type of defect. Figs. 22-25 shows the signals of the transmitted A_0 wave and converted S_0 wave received at the measurement point B from the FE simulation of incident A_0 wave propagating through welded joints with the defects of root crack, lack-of-penetration, porosity and lack-of-fusion, respectively, while Fig. 26 shows the comparison of the received signals from the FE simulation of the incident A_0 wave propagating through the mild steel and austenitic stainless steel plates with the welded joints. Similar conclusions as discussed in Section 4.2 on S_0 wave incident can be applicable to many defect cases for A_0 wave incident. However, it is worth mentioning that for the lack-of-penetration and lack-of-fusion cases, the transmitted A_0 wave signals seem to experience some deconstructive interference as shown in Figs. 23(a) and 25(a). This may be attributed to their irregular cross-section shape of the defects. In other words, the inclined angle of defect or trapezoidal shape discontinuity could have significant impacts on the transmitted signals of A_0 guided waves.

5. Parametric studies

In this section, the influence of several basic parameters for various types of weld defects on the transmission behaviour of incident S_0 and A_0 guided waves is studied quantitatively. To develop damage detection strategy in welded joint of steel plate, scanning of a healthy welded plate in pulse transmission mode at selected modes is firstly performed to obtain the baseline signals, followed by the recording of the ultrasonic signals of the plates with weld defects. Hence, the transmission coefficient, which is defined as the ratio of the maximum amplitude of signal envelope of transmitted guided wave propagating through weld defects to the maximum amplitude of signal envelope of incident guide wave propagating through healthy welded joint, will be adopted as a critical indicator for identifying the transmission performance of the ultrasonic guided waves for damage detection. In this parametric study, the material properties and geometric dimensions of the mild steel plate and welded joints, the ultrasonic testing set-up, the excitation frequency and the wave envelope calculation are considered to be the same as those described in Section 4 on mode conversion and scattering analysis.

5.1 Toe and root cracks

As is discussed in Section 4, the transmitted S_0 wave signals in the steel plate for the toe crack and root crack

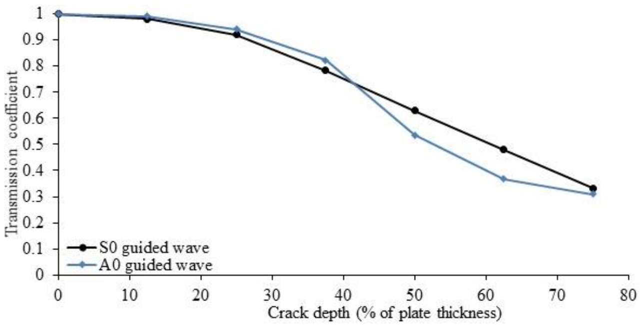

Fig. 27 Effect of variation of crack depth on transmission coefficient of S_0 and A_0 guided waves

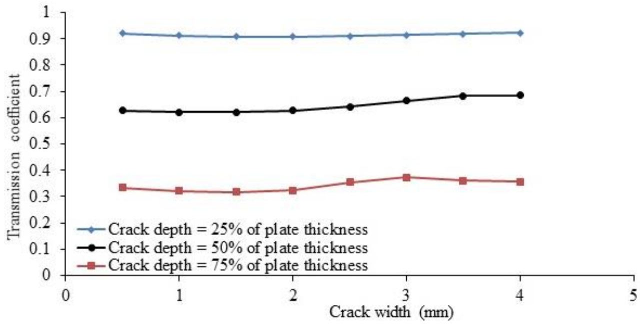

Fig. 28 Effect of variation of crack width on transmission coefficient of S_0 guided wave

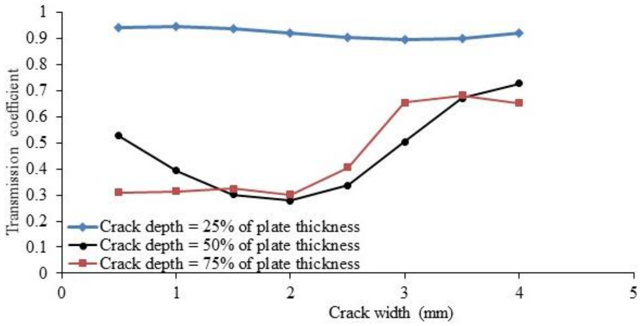

Fig. 29 Effect of variation of crack width on transmission coefficient of A_0 guided wave

cases are almost identical when the geometric dimensions of the simulated toe crack and root crack are the same. Therefore, only the toe crack is considered in this study. Fig. 27 shows the effect of the change in crack depth on the transmission coefficient for incident S_0 and A_0 guided waves. The crack depth h_c is varied from 0 to 3 mm corresponding to 0 to 75% of plate thickness while the crack width w_c remains constant at the 0.5 mm. It can be seen that as the crack depth increases, the transmission coefficients of S_0 and A_0 waves decrease monotonically. When the crack depth is incremented to 12.5% of the plate thickness, the transmission coefficients of both mode waves are marginally affected. But as the crack grows deeper to 50% of the plate thickness, the fall in the transmission ratios becomes steeper for both mode waves. This trend is consistent with the experimental results reported in the literature (Sharma and Mukherjee 2014) although that presented the study of notch detection in a submerged steel plate. Figs. 28 and 29 depict the effect of the change in crack width on the transmission coefficient for incident S_0 and A_0 waves, respectively. Eight different crack widths from 0.5 mm to 4 mm are studied for each crack depth case. Three crack depths, 25%, 50% and 75% of plate thickness, were chosen for the case study. The effect of the variation of crack inclined angle on the transmission coefficient of S_0 and A_0 waves is shown in Fig. 30. In practice, crack defects could be oriented at an arbitrary angle to the surface of the plate as is shown in Fig. 31. Different inclined angles θ_c from 0° to 45° are selected in the study. Apparently, the influence of the change in the crack width and crack inclined angle on the transmission coefficient of S_0 wave is not significant, because the crack width w_c of straight sided crack or the covered width w_{cover} of inclined crack is much smaller than the wavelength of S_0 waves as the theoretical wavelengths of S_0 waves with 300 kHz excitation frequency in 1, 2, 3 and 4 mm thick steel plates are approximately 17.8 mm. This observation is consistent with the findings in

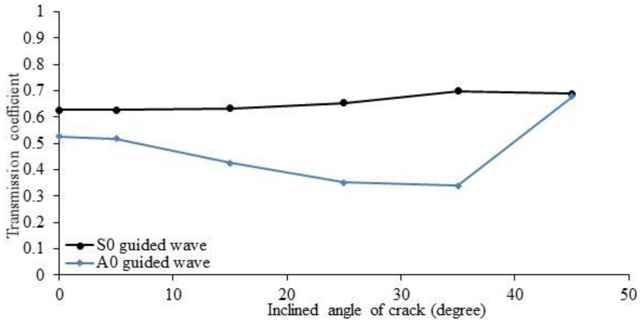

Fig. 30 Effect of variation of crack inclined angle on transmission coefficient of S_0 and A_0 guided waves

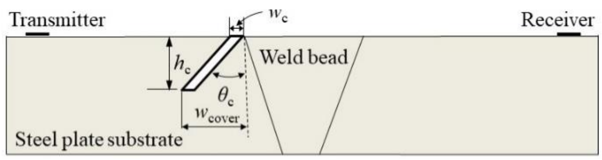

Fig. 31 Schematic diagram of cross-section of welded joint with inclined toe-crack

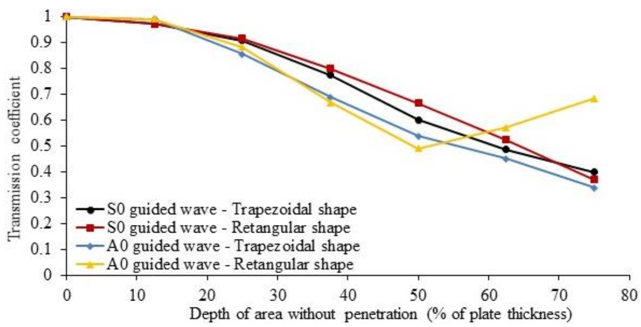

Fig. 32 Effect of variation in depth of area without weld penetration on transmission coefficient of S_0 and A_0 guided waves

the reference (Alleyne and Cawley 1992).

On the other hand, the change in the crack width and crack inclined angle produce substantial influences on the transmission coefficient of the A_0 wave. As is shown in Fig. 29, although the variation of the transmission coefficient of A_0 wave caused by the change of crack width is marginal when the crack depth is 25% of plate thickness, the oscillated changing of the transmission coefficient of A_0 wave caused by the change of crack width are recognised for the cases of crack depth being 50% and 75% of the plate thickness. Take the 50% of plate thickness crack depth case as an example. The transmission coefficient starts at a value of 0.53 when the crack width w_c is quite small as 0.5 mm, then decreases as the crack width is increased. The lowest value of the transmission coefficient as 0.28 occurs when the notch width is around 2 mm. Subsequently, the transmission coefficient rises with an increase of crack width until reaching a high value when the crack width is 4 mm. A similar pattern of the variation of transmission coefficient of A_0 wave related with the change of crack width is observed for 75% of the plate thickness crack width case, except that the lowest and highest point take places when the crack width is around 1 and 3.5 mm, respectively. The reason of this oscillation could be the interference between two A_0 wave signals with different waveforms occurring at the crack region. At the crack region, the thickness of the plate is reduced. Another A_0 wave with different waveform and wavelength is generated in the crack region or known as the thickness-reduced plate region. The new generated A_0 wave and the original A_0 waves are superposed and results in the transmitted A_0 wave packet but the superposition in the resulting transmitted wave packet may be constructive or destructive. As is calculated, the theoretical wavelengths of A_0 waves with 300 kHz excitation frequency in 1, 2, 3 and 4 mm thick steel plates are 5.1, 6.6, 7.6 and 8.2 mm, respectively. Hence, it can be estimated the minimum of transmission coefficient is reached when the crack width is about 60% of half of the wavelength of the A_0 wave in the thickness-reduced plate and the maximum of the transmission coefficient is attained when the crack width is about 60% of the full wavelength of the A_0 wave in the thickness-reduced plate. The reason for the fact that the maximum and minimum of the transmission coefficient don't occur precisely at the half and full wavelength positions could be attributed to the contributions of those anti-symmetric mode wave packets generated following the incident A_0 wave mentioned in Section 3.3. It can be concluded that, the variation of the transmission coefficient of S_0 wave in the welded steel plate with toe or root crack is largely dependent on the change of crack depth while the variation of the transmission coefficient of A_0 wave have close correlation with the changes of both the crack depth and crack width.

5.2 Lack-of-penetration, porosity and lack-of-fusion

Fig. 32 shows the effect of the change in the depth of area without weld penetration on the transmission coefficient of S_0 and A_0 waves. Two kinds of shapes of cross-section of area without weld penetration are considered to illustrate their effect on the transmission coefficient. The trapezoidal shape cross-section is shown in Fig. 10(c) while the rectangular shape cross-section is like that of the root crack (Fig. 10(b)) with the width being equal to the bottom width of the weld bead as 3 mm. The depth of the lack-of-penetration area h_{pe} is varied from 0 to 3 mm corresponding to 0 to 75% of the plate thickness. Because the lack-of-penetration defect is defined as notch-like discontinuity at the welded joint, a similar observation discussed in Section 5.1 on the notch-like toe crack could be found on the lack-of-penetration defect. The transmission coefficients of S_0 waves reduce monotonically as the depth of area without weld penetration increases. The change of the shape of cross-section of area without weld penetration has limited influence on the transmission coefficients of S_0 waves but significantly affects the transmission coefficients of A_0 waves due to the interference phenomenon of A_0 wave signals at the weld defect region.

Porosity and lack-of-fusion are regarded as two types of internal defects. Fig. 33 shows the effect of the variation of porosity position on the transmission coefficient of S_0 and A_0 waves. The diameter of circular porosity void D_{po} is assumed to be 1 mm and the distance between the centre of the void and the plate surface h_{po} is varied from 0 to 2 mm corresponding to 0 to 50% of the plate thickness. Apparently, both the S_0 and A_0 waves are insensitive to this type of internal defect when its size is small wherever they are located. Fig. 34 shows the effect of the variation of size of porosity on the transmission coefficient of S_0 and A_0 waves. The centre of circular porosity void is positioned at

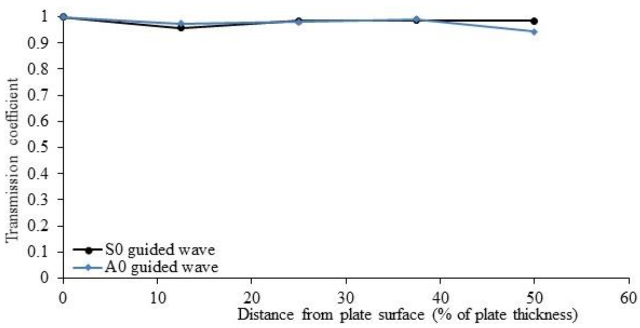

Fig. 33 Effect of variation of porosity position on transmission coefficient of S_0 and A_0 guided waves

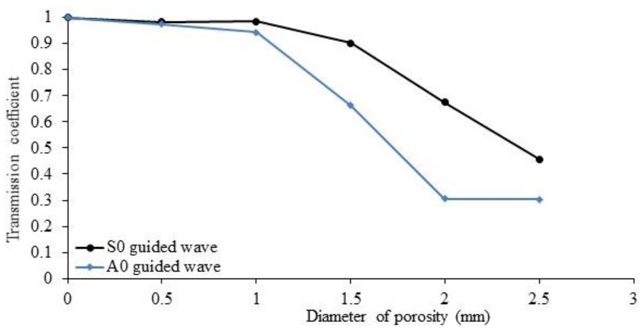

Fig. 34 Effect of variation of porosity size on transmission coefficient of S_0 and A_0 guided waves

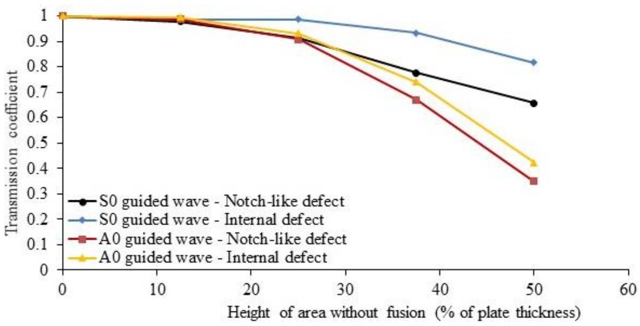

Fig. 35 Effect of variation in height of area without fusion on transmission coefficient of S_0 and A_0 guided waves

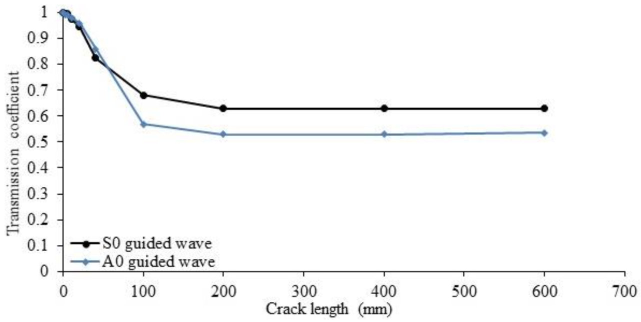

Fig. 36 Effect of variation of defect length on transmission coefficient of S_0 and A_0 guided waves

the mid-thickness point of the plate and six different diameters of void from 0 to 2.5 mm is selected. Overall, the transmission coefficient of S_0 and A_0 wave decreases with an increase of the diameter of porosity, even though the decrease is negligible when the diameter drops from 0 to 1 mm. There is also oscillation on the curve of A_0 wave which could be also caused by the interference effect of the A_0 wave signals.

Fig. 35 shows the effect of the change in the height of lack-of-fusion defect on the transmission coefficient of S_0 and A_0 waves. To compare the sensitivity of S_0 and A_0 waves to the notch-like defect and internal defect, the models with two kinds of lack-of-fusion defects are analysed. One is with an inclined internal discontinuity as shown in Fig. 10(e) and the other one is with an inclined notch-like crack located at the surface of weldment to the base material substrate. The width w_f of both types of defect is 0.5 mm and the height h_f are varied from 0 to 2 mm corresponding to 0 to 50% of the plate thickness. It is shown that the transmission coefficient decreases with an increase of the height of lack-of-fusion defect for both S_0 and A_0 waves. The S_0 wave is more sensitive to the notch-like defect than to the internal defect since the transmission coefficient of S_0 wave propagating the notch-like defect reduce more dramatically than the one for S_0 wave propagating the internal defect, while the sensitivity of A_0 wave to these two kinds of defects is quite similar.

5.3 Effect of defect length

In the previous subsections, all the defects are assumed to have a full length being cut through the full width of the plate along the welding direction and normal to the transmission path. Investigation of the effects of the defect lengths on the transmission coefficient of S_0 and A_0 waves are described in this subsection. The analysis is performed for different defect lengths viz l = 2, 5, 10, 20, 50, 100, 200, 400 and 600 (full length) mm. Fig. 36 shows the variation of the transmission coefficient of S_0 and A_0 waves due to the change of the length of toe crack (w_c = 0.5 mm and h_c = 2 mm). When the crack length is less than 100 mm, the transmission coefficient of both mode waves go down dramatically as the crack length is extended. The larger portion of the incident mode waves striking the crack results in a smaller value of transmission coefficient. However, when the crack length is extended to more than 100 mm, the effect of the crack length on the transmission coefficient is degraded significantly and the transmission coefficient approaches to a value corresponding to the cases of the crack length being equal to the full length. It can be concluded that the change of crack length indeed produces an impact on the transmission coefficient of S_0 and A_0 waves when the crack length is relatively small.

6. Conclusions

This paper has presented an investigation of the transmission characteristics of ultrasonic guided waves propagating through weld defects in steel plates with welded joints. The research focused on studying the behaviour of the fundamental symmetric (S_0) and anti-symmetric mode (A_0) guided waves. A 3D explicit FE model based on the pulse transmission ultrasonic testing set-up in which the transmission path is perpendicular to the longitudinal direction of weld bead was developed for this investigation. The FE model considered the constraint conditions between the interfaces of the weldment and the steel plate component. Different material properties of the mild steel plate, austenitic stainless steel plate and their corresponding welded joints were taken into account in the model. The FE model was verified against the semi-analytical results of dispersion curves and the experimental results of ultrasonic guided wave testing in steel plates with notches and was shown to be able to accurately simulate the guided wave propagation in steel plate with welded joint.

Invoking the validated FE model, the mode conversion and scattering characteristics of the S_0 and A_0 guided waves transmitted at welds defects in the steel plates with welded joints were illustrated. Five types of common weld defects, toe crack, root crack, lack-of-penetration, porosity and lack of fusion, were taken into consideration. The results showed when the S_0 and A_0 guided waves interact with the weld defect, they undergo mode conversion. Two propagating modes of waves including the transmitted S_0 wave and converted A_0 wave were generated after the incident S_0 wave interacting with weld defect while the transmitted A_0 wave and converted S_0 wave were generated after the interaction between the incident A_0 wave and the weld defect. The waveform of signals of the transmitted and converted waves were shown to be affected by the types of weld defects. But the influence of the elastic anisotropy of austenitic welds on the signal waveform were marginal as only small phase shifts and amplitude change on the received time-domain signal output were observed, which highlights the advantage of using ultrasonic guided waves for weld defect detection in austenitic stainless steel plate compared with the use of ultrasonic bulk wave.

Parametric studies were then undertaken by using the FE model to elucidate the effects of several basic parameters for various types of weld defects on the transmission performance for incident S_0 and A_0 guided waves. The transmission coefficient was introduced as an indicator for identifying the transmission performance of guided waves. It was shown that the influence of the depth of crack and lack-of-penetration defect, the size of porosity and the height of lack-of-fusion defect on the transmission coefficient of S_0 waves was significant. The transmission coefficient of S_0 waves decreased monotonically with an increase of these parameters for each kind of weld defect case. While the effects of the width and inclined angle of crack and the shape of cross-section of lack-of-penetration defect on the transmission coefficient of S_0 waves were little. The variation of the transmission coefficient of S_0 wave was more sensitive to the change of the height of notch-like defect than to that of internal defect, and was affected by the change of the defect length along the welding direction. For A_0 wave, the transmission coefficient was influenced by the complex correlation of most of the basic parameters for different types of weld defects because of the interference phenomenon of A_0 wave signals at the weld defect region. Therefore, it can be suggested that the application of the transmission of S_0 guided waves could be an ideal solution for defect detection in welded joints of steel plates and the application of the transmission of A_0 guided waves could be an attractive supplemental tool for sizing the defects. The finding of this study advances the further development of damage detection technologies for weld inspection. Future work could be carried out to establish an artificial neural network for damage detection in welded joints of steel plates based on the transmission coefficient, in which other parameters such as the height of weld cap, the combination of weld defects, the positions of guided wave transmitter and receiver, the signal excitation frequency and the steel plate thickness will be taken into account.

Acknowledgments

The research described in this paper was financially supported by the the Australia Research Council through Linkage Project (LP150100475) awarded to the second and third author. This support is gratefully acknowledged.

References

Alleyne, D. and Cawley, P. (1991), "A two-dimensional Fourier transform method for the measurement propagating multimode signals", *J. Acoust. Soc. Am.*, **89**, 1159-1168. https://doi.org/10.1121/1.400530

Alleyne, D.N. and Cawley, P. (1992), "The interaction of Lamb waves with defects", *IEEE Transactions on Ultrasonics, Ferroelectrics, and Frequency Control*, **39**(3), 381-397. https://doi.org/10.1109/58.143172

AS/NZS 1554.1 (2014), Structural steel welding Part 1: Welding of steel structures, Standards Australia (SA); Sydney, Australia.

AS/NZS 1554.4 (2014), Structural steel welding Part 4: Welding of high strength quenched and tempered steels, Standards Australia (SA); Sydney, Australia.

AS/NZS 1554.6 (2012), Structural steel welding Part 6: Welding stainless steels for structural proposes, Standards Australia (SA); Sydney, Australia.

Bathe, K.J. (1982), *Finite Element Procedures in Engineering Analysis*, Prentice-Hall, Englewood Cliffs, New Jersey, USA.

Cawley, P. and Alleyne, D.N. (1996), "The use of Lamb waves for the long range inspection of large structures", *Ultrasonics*, **34**, 287-290. https://doi.org/10.1016/0041-624X(96)00024-8

Choi, Y. and Kwon, Y.B. (2018), "Direction strength method for high strength steel welded section columns", *Steel Compos. Struct., Int. J.*, **29**(4), 509-526. https://doi.org/10.12989/scs.2018.29.4.509

Consonni, M., Wee, C.F. and Schneider, C. (2012), "Manufacturing of welded joints with realistic defects", *Insight: Non-Destructive Testing and Condition* Monitoring, **54**(2), 76-81. https://doi.org/10.1784/insi.2012.54.2.76

Ding, F.X., Yin, Y.X., Wang, L., Yu, Y., Luo, L. and Yu, Z.W. (2019), "Confinement coefficient of concrete filled square stainless steel tubular stub columns", *Steel Compos. Struct., Int. J.*, **30**(4), 337-350. https://doi.org/10.12989/scs.2019.30.4.337

Ditchburn, R.J., Burke, S.K. and Scala, C.M. (1996), "NDT of weld: state of the art", *NDT&E International*, **29**(2), 111-117. https://doi.org/10.1016/0963-8695(96)00010-2

Fan, Z. and Lowe, M.J.S. (2012), "Interaction of weld-guided waves with defects", *NDT & E International*, **47**, 124-133. https://doi.org/10.1016/j.ndteint.2012.01.001

Gravenkamp, H., Prager, J., Saputra, A.A. and Song, C. (2012), "The simulation of Lamb waves in a cracked plate using the scaled boundary finite element method", *J. Acoust. Soc. Am.*, **132**, 1358-1367. https://doi.org/10.1121/1.4740478

Halmshaw, R. (1997), *Introduction to the Non-Destructive Testing of Welded Joints*, Woodhead Publishing, Cambridge, England.

Hellier, C. and Shakinovsky, M. (2012), *Handbook of Non-Destructive Evaluation*, McGraw-Hill Education, New York, NY, USA.

Hibbit, H.D., Karlsson, B.I. and Sorensen, E.P. (2016), *ABAQUS 2016 User's Manual*, Hibbitt, Karlsson & Sorensen Inc, Pawtucket, RI, USA.

Huang, Z., Li, D., Uy, B., Thai, H.T. and Hou, C. (2019), "Local and post-local buckling of fabricated high-strength steel and composite columns", *J. Constr. Steel Res.*, **154**, 235-249. https://doi.org/10.1016/j.jcsr.2018.12.004

Joo, H.S., Moon, J., Sung, I.-H. and Lee, H.-E. (2015), "Moment redistribution of continuous composite I-girder with high strength steel", *Steel Compos. Struct., Int. J.*, **18**(4), 873-887. https://doi.org/10.12989/scs.2015.18.4.873

Juluri, N., Lowe, M. and Cawley, P. (2007), "The guiding of ultrasound by a welded joint in a plate", *AIP Conference Proceedings*, **894**, 1079-1086. https://doi.org/10.1063/1.2718087

Kamas, T., Giurgiutiu, V. and Lin, B. (2015), "Quasi-Rayleigh waves in butt-welded thick steel plate", *AIP Conference Proceedings*, **1650**, 686-694. https://doi.org/10.1063/1.4914669

Kundu, T. (2016), *Ultrasonic and Electromagnetic NDE for Structure and Material Characterization: Engineering and Biomedical Applications*, CRC Press, New York, NY, USA.

Li, D., Uy, B., Aslani, F. and Hou, C. (2019), "Behaviour and design of spiral-welded stainless steel tubes subjected to axial compression", *J. Constr. Steel Res.*, **154**, 67-83.

Lian, M., Su, M. and Guo Y. (2015), "Seismic performance of eccentrically braced frames with high strength steel combination", *Steel Compos. Struct., Int. J.*, **18**(6), 1517-1539. https://doi.org/10.12989/scs.2015.18.6.1517

Lian, M., Su, M. and Guo, Y. (2017), "Experimental performance of Y-shaped eccentrically braced frames fabricated with high strength steel", *Steel Compos. Struct., Int. J.*, **24**(4), 441-453. https://doi.org/10.12989/scs.2017.24.4.441

Lowe, M.J.S. and Diligent, O. (2002), "Low-frequency reflection characteristics of the S_0 Lamb wave from a rectangular notch in a plate", *J. Acoust. Soc. Am.*, **111**, 64-74. https://doi.org/10.1121/1.1424866

Lowe, M.J.S., Cawley, P., Kao, J.-Y. and Diligent, O. (2002), "The low frequency reflection characteristics of the fundamental antisymmetric Lamb wave a_0 from a rectangular notch in a plate", *J. Acoust. Soc. Am.*, **112**, 2612-2622. https://doi.org/10.1121/1.1512702

Lu, X., Lu, M., Zhou, L.-M., Su, Z., Cheng, L., Ye, L. and Meng, G. (2011), "Evaluation of welding damage in welded tubular steel structures using guided waves and a probability-based imaging approach", *Smart Mater. Struct.*, **20**, 1-15. https://doi.org/10.1088/0964-1726/20/1/015018

Marzani, A., Viola, E., Bartoli, L., Lanza Di Scalea, F. and Rizzo, P. (2008), "A semi-analytical finite element formulation for modelling stress wave propagation in axisymmetric damped waveguides", *J. Sound Vib.*, **318**, 488-505. https://doi.org/10.1016/j.jsv.2008.04.028

Moreau, L. and Castaings, M. (2008), "The use of an orthogonally relation for reducing the size of finite element models for 3D guided waves scattering problem", *Ultrasonics*, **48**(5), 357-366. https://doi.org/10.1016/j.ultras.2008.01.005

Murta, R.H.F., Vieira, F.D.A., Santos, V.O. and de Moura, E.P. (2018), "Welding defect classification from simulated ultrasonic signals", *J. Nondestructive Eval.*, **37**(3), 40. https://doi.org/10.1007/s10921-018-0496-y

Rose, J.L. (2014), *Ultrasonic Guided Waves in Solid Media*, Cambridge University Press, New York, NY, USA.

Sargent, J.P. (2006), "Corrosion detection in welds and heat-affected zones using ultrasonic Lamb waves", *Insight: Non-Destructive Testing and Condition Monitoring*, **48**(3), 160-167. https://doi.org/10.1784/insi.2006.48.3.160

Serey, V., Quaegebeur, N., Micheau, P., Masson, P., Castaings, M. and Renier, M. (2018), "Selective generation of ultrasonic guided waves in a bi-dimensional waveguide", *Struct. Health Monitor.*, 1475921718808220. https://doi.org/10.1177/1475921718808220

Sharma, S. and Mukherjee, A. (2014), "A non-contact technique for damage monitoring in submerged plates using guided waves", *J. Test. Eval.*, **43**(4), 776-791. https://doi.org/10.1520/JTE20120357

Soleimanpour, R. and Ng, C.-T. (2015), "Mode conversion and scattering analysis of guided waves at delaminations in laminated composite beams", *Struct. Monitor. Maint., Int. J.*, **2**(3), 213-236. https://doi.org/10.12989/smm.2015.2.3.213

Soleimanpour, R. and Ng, C.-T. (2016), "Scattering of the fundamental anti-symmetric Lamb wave at through-thickness notches in isotropic plates", *J. Civil Struct. Health Monitor.*, **6**(3), 447-459. https://doi.org/10.1007/s13349-016-0166-7

Staszewski, W.J., Boller, C. and Tomlinson, G.R. (2004), *Health Monitoring of Aerospace Structures: Smart Sensor Technologies and Signal Processing*, Wiley, New York, NY, USA.

Stavridis, J., Papacharalampopoulos, A. and Stavropoulos, P. (2018), "Quality assessment in laser welding: a critical review", *Int. J. Adv. Manuf. Technol.*, **94**(5-8), 1825-1847. https://doi.org/10.1007/s00170-017-0461-4

Stewart, J.R., Gullerud, A.S. and Heinstein, M.W. (2006), "Solution verification for explicit transient dynamics problems in the presence of hourglass and contact forces", *Comput. Methods Appl. Mech. Eng.*, **195**, 1499-1516. https://doi.org/10.1016/j.cma.2005.05.043

Su, Z. and Ye, L. (2009), *Identification of Damage Using Lamb Waves: From Fundamentals to Applications*, Springer Science & Business Media, London, England.

Theofanous, M., Saliba, N., Zhao, O. and Gardner, L. (2014), "Ultimate response of stainless steel continuous beams", *Thin-Wall. Struct.*, **83**, 115-127. https://doi.org/10.1016/j.tws.2014.01.019

Yang, L. and Ume, C. (2017), "Measurement of weld penetration depths in thin structures using transmission coefficients of laser-generated Lamb waves and neural network", *Ultrasonics*, **78**, 96-109. https://doi.org/10.1016/j.ultras.2017.02.019

Yang, L., Wang, Y., Gao, B., Shi, Y. and Yuan, H. (2014), "Two calculation methods for buckling reduction factors of stainless steel welded I section beams", *Thin-Wall. Struct.*, **83**, 128-136. https://doi.org/10.1016/j.tws.2014.01.012

Yang, Y., Ng, C.-T. and Kotousov, A. (2019), "Second harmonic generation of guided wave at crack-induced debonding in FRP-strengthened metallic plates", *Int. J. Struct. Stabil. Dyn.*, **19**(1), 1940006. https://doi.org/10.1142/S0219455419400066

Yuan, H.X., Wang, Y.Q., Gardner, L. and Shi, Y.J. (2014), "Local-overall interactive buckling of welded stainless steel box section compression members", *Eng. Struct.*, **67**, 62-76. https://doi.org/10.1016/j.engstruct.2014.02.012

Zhang, L., Luo, W. and Rose, J.L. (2006), "Ultrasonic guided wave focusing beyond welds in a pipeline", *AIP Conference Proceedings*, **820**, 877-884. https://doi.org/10.1063/1.2184618

Zhou, H., Han, Z., Du, D. and Chen, Y. (2018), "A combined marching and minimizing ray-tracing algorithm developed for ultrasonic array imaging and austenitic welds", *NDT & E International*, **95**, 45-56. https://doi.org/10.1016/j.ndteint.2018.01.008

Zuo, P., Yu, X. and Fan, Z. (2017), "Numerical modeling of embedded solid waveguides using SAFE-PML approach using a commercially available finite element package", *NDT & E International*, **90**, 11-23. https://doi.org/10.1016/j.ndteint.2017.04.003

DL